Elaboration of Porous Alumina Nanofibers by Electrospinning and Molecular Layer Deposition for Organic Pollutant Removal

Petros Abi Younes, Syreina Sayegh, Amr Nada, Matthieu Weber, Igor Iatsunskyi, Emerson Coy, Nadine Abboud, Mikhael Bechelany

Elaboration of Porous Alumina Nanofibers by Electrospinning and Molecular Layer Deposition for Organic Pollutant Removal

Petros Abi Younes[1,2], Syreina Sayegh [1], Amr A. Nada [1,3], Matthieu Weber [1,2] , Igor Iatusnkyi [4], Emerson Coy [4], Nadine Abboud [5] and Mikhael Bechelany [1,*]

1 Institut Européen des Membranes, IEM, UMR 5635, Univ Montpellier, ENSCM, CNRS, 34730 Montpellier, France
2 Université Grenoble Alpes, CNRS, Grenoble INP, LMGP, 38400 Grenoble, France
3 Department of Analysis and Evaluation, Egyptian Petroleum Research Institute, Cairo, Nasr City P.B. 11727, Egypt
4 NanoBioMedical Centre, Adam Mickiewicz University, Wszechnicy Piastowskiej 3, 61-614 Poznan, Poland
5 LPA, Faculty of Science 2, Fanar Campus, Lebanese University, Fanar B.P. 90656, Lebanon
***** Correspondence: mikhael.bechelany@umontpellier.fr

Abstract

The development of heterogeneous nanomaterials with high surface to volume ratio is crucial for enhancing the adsorption of water pollutants, such as toxic organic dyes. Here, we describe the synthesis of polyacrylonitrile (PAN) nanofibers coated with porous alumina nanolayers, and their application for adsorption of the organic dye methylene blue (MB). First, we produced PAN nanofibers by electrospinning, and then coated them with an aluminum alkoxide hybrid films fabricated using molecular layer deposition. Finally, we used thermal annealing to obtain the final PAN nanofibers coated with porous alumina nanolayers. We characterized the obtained nanostructured materials by scanning electron microscopy, transmission electron microscopy, N_2 desorption/adsorption porosimetry (BET theory), and Fourier-transform infrared spectroscopy. The porous nanomaterials had a surface area of 631.79 m^2/g that allowed reaching an adsorption efficiency of 88% with 10 ppm MB. The adsorption kinetics and isotherms were better described by a pseudo-first-order model and the Langmuir adsorption model, respectively, based on physical adsorption (monolayer adsorption) of the adsorbed molecules.

Key words: water treatment, adsorption, alucone, mesoporous materials, nanofibers, ALD/MLD.

Introduction

Effectual removal of organic pollutants from polluted waters is a crucial step towards a sustainable environment. Wastewater produced by the dye industry[1] is a major contributor to water pollution. Many strategies have been tested for removing such dyes from wastewaters, for instance ultrasound oxidation, biological removal, membranes-based separation, photocatalytic degradation[2] and adsorption[3,4].

Adsorption is considered as the most effective approach in wastewater treatment due to its low cost, simple design, flexibility, operation simplicity, and insensitivity to toxic pollutants. [5] Adsorption process consists on transferring the organic dye to the surface of solid and very porous particles (i.e. adsorbents)[6,7], such as nano-sized materials with elevated porosity, surface area-to-volume ratio, and regeneration potential[8–11]. Among these nanomaterials, nanofibers are excellent candidate adsorbents due to their high surface area and tunable porosity, 3D topography, flexible surface functionalities, mechanical features, and small pore diameter and consequently higher number of active sites for contaminant adsorption. Nanofibers have been widely studied for air and water filtration and for blood purification[12], particularly porous alumina nanofibers. This nanomaterial is easy to handle and presents high surface area and very good thermal stability and tensile strength, due to the sub-micrometer and tunable pore size[13,14]. Alumina nanofibers can be manufactured using various techniques: hydrothermal growth[15], solvothermal growth [16], chemical vapor deposition[17] and electrospinning[18,19].

Here we are reporting the elaboration of porous alumina nanofibers by combining electrospinning and Molecular Layer Deposition (MLD) for organic pollutant removal. Electrospinning, a low-cost method in which electrostatic forces are the driving force, is frequently chosen for nanofiber manufacturing.[20,21] Among the used polymer for electrospinning, polyacrylonitrile (PAN) was used as a substrate for depositing thin films materials, due to its stable synthetic polymeric nature that can be easily electrospun into nanofiber. On the other hand, PAN was largely used in the literature as a substrate, since it can be completely removed upon annealing under air at high temperatures allowing to obtain nanotubes structures [22,23].

For the deposition of thin film on PAN nanofibers, Atomic Layer Deposition (ALD) and Molecular Layer Deposition (MLD) have been chosen in this work. ALD is a gas phase growth technique based on sequential self-limiting surface reaction of precursor's injections into the reaction chamber

separated by an inert gas as purge step. The chemical adsorption of the precursors vapor during surface reaction permits to obtain a stable covalent bonds and ensures that thin films are bonded to the substrate. That is why ALD process can be used to coat high aspect-ratio substrates and complex 3D-structures such as polymers, ceramics and metals.[24] The high-quality thin films obtained by ALD shows excellent conformality and thickness control[25]. Therefore, ALD has been used for various applications, including water pollution remediation[26–29]. MLD is a novel method directly derived from ALD[30]. The two techniques are based on sequential and self-limiting surface reactions for the preparation of functional coatings.

Aluminum alkoxide (alucone) hybrid polymer films can be deposited on nanofibers using MLD and suitable precursors, such as trimethylaluminum (TMA) and ethylene glycol (EG). MLD-based deposition of dense organic/inorganic hybrid polymer films is followed by thermal annealing to remove the organic template and to obtain well-defined porous structures with precisely controlled thickness, in the Ångstroms range[31,32]. MLD-based addition of thin porous films to the surface of nanomaterials can lead to new surface functionalities.[33,34]

In this work, a new fabrication route for porous alumina nanofiber based on combining both electrospinning and Molecular Layer Deposition were presented. The synthesized polyacrylonitrile (PAN) nanofibers by electrospinning, were coated by alucone using MLD. Then the organic template was removed by calcination, allowing to obtain a porous nanofibers structure with high surface area. The high surface area is the driving force to adsorption studies on the removal of organic dyes. A comparative study between MLD and ALD was performed after annealing, showing a porous aluminum oxide (**p Al_2O_3**) and dense aluminum oxide (**d Al_2O_3**) films, respectively. The high surface area values resulting from the **p Al_2O_3** comparing to the **d Al_2O_3** showed the novelty aspect to deposit by MLD process. This was evaluated by adsorption study on the removal of methylene blue (MB) dye from aqueous solutions.

2. Experimental

2.1. Chemicals

PAN (MW = 500 000, Sigma Aldrich) and *N,N*-dimethylformamide (DMF, CAS number 68-12-2, 99.8%, Sigma Aldrich) were used to fabricate the PAN nanofibers. Alucone polymer films were grown using TMA ($Al(CH_3)_3$; 97%, Sigma Aldrich) and EG ($HO(CH_2)_2OH$; Reagent Plus >99%, Sigma Aldrich). MB (Reagent Plus >82.0%) (Sigma-Aldrich) was the reference organic dye.

2.2. Synthesis of alucone/PAN and Al_2O_3/PAN nanofibers

2.2.1. PAN nanofibers

PAN nanofibers were produced by electrospinning. The polymer solution was prepared by dissolving PAN in DMF (2mg PAN in 18 mL DMF) by stirring at 60°C for 24 hours, and then was loaded into a plastic syringe with a stainless steel needle[35]. Electrospinning (applied voltage: 25 kV; flow rate: 3 mL/h; needle tip-collector distance: 15 cm) was performed at 38 ± 5°C to evaporate the solvent and to obtain solid fibers on the collector. Nanofibers were collected on a rotating cylinder (10 cm diameter and rotating speed of 2000 rpm) covered with aluminum foil. The process lasted 7h.

2.2.2. MLD of alucone on PAN nanofibers

MLD of aluminum alkoxide (alucone) thin films were deposited over PAN nanofibers[36] using a home-built ALD/MLD system. The process was obtained using TMA and EG as precursors. The EG precursor bubbler was heated at 70 °C while the TMA bubbler was maintained at room temperature. The deposition chamber was maintained at 135°C during the process and precursors line was kept at 100°C. The precursor pulses were coupled with a 10 sccm Argon (Ar) flow. MLD was carried out using an exposure mode to obtain the self-limiting surface reaction and by-products were pumped using a 100 sccm Argon (Ar) flow as gas vector during purge. Each MLD cycle (250 cycles in total) consisted of a TMA pulse for 0.1s, exposure for 30s, purge for 60s, EG pulse for 2s, exposure for 30s and purge for 120s.

2.2.2. ALD of Al_2O_3 on PAN nanofibers

Al_2O_3 thin films were deposited on PAN nanofibers by ALD using TMA and H_2O as precursors. The films were grown in a deposition chamber at 60°C. The precursor pulses were coupled with a 25

sccm Argon flow and the purge step was performed with a 100 sccm Argon flow. Each ALD cycle (50 cycles in total) consisted of a TMA pulse for 0.2s, exposure for 30s, purge for 40s, H_2O pulse for 2s, exposure for 30s, and purge for 40s.

2.2.3. Calcination in air

To convert the alucone nanofilms prepared by MLD into porous alumina (p Al_2O_3), the nanomaterial was calcined in air in a muffle oven at 600 °C with a ramp rate of 1°C/min. Then, the temperature was maintained at 600 °C for 1h before starting the cooling step.

The same process was used also for the samples prepared by ALD (i.e. PAN nanofibers coated by Al_2O_3 films to convert the Al_2O_3 into dense Al_2O_3 (d Al_2O_3)).

2.3. Characterization

The morphology and structure of the synthesized materials was examined by scanning electron microscopy (SEM) (ZEISS EVO HD-15, ZEISS, Marly le Roi, France) and high-resolution transmission electron microscopy (HR-TEM, JEOL ARM 200F, Japan) with an energy dispersive X-ray (EDX) analyzer. X-ray diffraction (XRD) was used to determine whether the deposited alumina is amorphous or crystalline after annealing (PANAlytical Xpert-PRO with Cu radiation at 0.154nm). The sample porosity was measured by N_2 desorption/adsorption porosimetry with degassing under vacuum at 300 ° C for 24h. The surface area was calculated with the Brunauer, Emmet and Teller (BET) method using different data points and relative pressures (P/Po) from 0.2 to 0.8. The Fourier-transform infrared spectroscopy (FT-IR) spectra of the samples dispersed in KBr pellets were recorded with a 670 FT-IR spectrometer (Varian) (400–4000 cm^{-1} range and resolution of 4 cm^{-1}). The thermogravimetric analysis (TGA) of the samples after calcination was performed using a TGA G500 device (TA Instruments). About 10 mg of each sample was heated in air atmosphere from room temperature to 800°C, at a heating rate of 10°C.min^{-1}. MB concentration was measured by ultraviolet-visible (UV–Vis) spectrophotometry (spectra acquired with a Jasco V-570 UV–Vis-NIR spectrophotometer (Jasco Inc., Easton, PA, USA), at λ = 664 nm, and the external calibration method.

2.4. Adsorption experiments

2.4.1. Batch equilibrium studies

MB (stock solution of 10 ppm) was used as organic pollutant reference to evaluate the adsorption performances of the prepared p Al_2O_3 and d Al_2O_3 samples. The adsorption test started with 0.01 g adsorbent and 5 mL of aqueous solution containing increasing MB concentrations (10, 15, 20, 25, and 30 ppm). The pH of the MB solution during the degradation was equal to 9 .The adsorbent-dye ratio was maintained at 2 g/L for both sample types. In the next experiment, using only p Al_2O_3/PAN, the adsorbent-dye ratio concentration was maintained at 4 g/L. Flasks were placed on a magnetic stirrer (400 rpm) at room temperature in the dark, and MB concentration was checked at different time points (0, 30, 60, 120 and 180 min) to assess MB adsorption. The adsorbent was separated from the dye solution after each adsorption experiment by centrifugation at 6000 rpm for 5 min. The UV–Vis absorbance spectra of the MB solution displayed a main adsorption band at 664 nm. Isothermal and kinetic analyses were performed (see below) to describe the adsorption process.

2.4.2. Adsorption isotherms

The adsorption behavior of an adsorbate onto an adsorbent can be quantitatively described using different adsorption isotherms. Here, the Langmuir and Freundlich models, two common theoretical models, were chosen to analyze the adsorption equilibrium process [37].

The Langmuir isotherm linear model assumes that a monolayer adsorption process occurs on the homogeneous surface of an adsorbent, without considering the interaction between adsorbate molecules. This model is described by Equation (1):

$$\mathbf{C_e/q_e = C_e/q_{max} + 1/q_{max}\, K_L} \quad \textbf{(Equation 1)}$$

where q_{max} (mg/g) and k_L (L/mg) are the Langmuir isotherm constants that describe the maximum adsorbed quantity and the free energy function of adsorption, respectively.

According to the Freundlich isotherm linear model, a multilayer adsorption process takes place on the non-homogeneous surface of an adsorbent. This model is described by Equation (2):

$$\ln q_e = \ln k_F + (1/n) \ln C_e \quad \text{(Equation 2)}$$

where the Freundlich isotherm coefficients K_F ((mg/g)(L/mg)1/n) and n are the adsorption capacity and adsorption intensity, respectively.

2.4.2. Adsorption kinetics

To determine the adsorption mechanism and the rate-controlling step of the adsorption process, the relationship between adsorbed quantity and sorption time were computed using pseudo first-order and pseudo second-order kinetic models. The control experiments for MB adsorption onto pAl_2O_3 were carried out in the same experimental conditions and simultaneously.

The linear equation of the pseudo first-order kinetic model is:

$$\log(q_e - q_t) = \log q_e - k_1 t / 2.303 \quad \text{(Equation 3)}$$

where q_t is the dye quantity (qt, mg/g) adsorbed onto the adsorbent at time t, and k_1 (1/min) is the kinetic rate constant of the pseudo first-order adsorption.

The linear equation of the pseudo second-order kinetic model is:

$$t/q_t = 1/k_2 q_e^2 + t/q_e \quad \text{(Equation 4)}$$

where K_2 (g/(mg.min)) denotes the rate constant of the pseudo second-order adsorption model.

3. Results and discussion

The nanofibers coated with a porous alumina layer (MLD; alucone/PAN) and with dense alumina layers (ALD; Al_2O_3/PAN) were first structurally and morphologically characterized.

3.1. Characterization of p Al_2O_3 and d Al_2O_3 nanofibers

3.1.1 Morphological properties of p Al_2O_3 and d Al_2O_3 nanofibers

SEM investigation of the surface morphology and microstructural properties of pAl_2O_3 and dAl_2O_3 deposited on PAN nanofibers used as substrate. After ALD/MLD deposition, the samples were calcinated at 600°C for 1h to ensure the elimination of the polymeric template. Figure 1 shows that well structured nanofibers were obtained in both cases after ALD (figure 1 a-b) and MLD

(figure 1 c-d) deposition. The mean diameters of the dAl_2O_3 films (ALD) and pAl_2O_3 layers (MLD) were =550 ± 10 nm (**Figure 1a-b**) and 460 ± 7nm (**Figure 1c-d**) respectively.

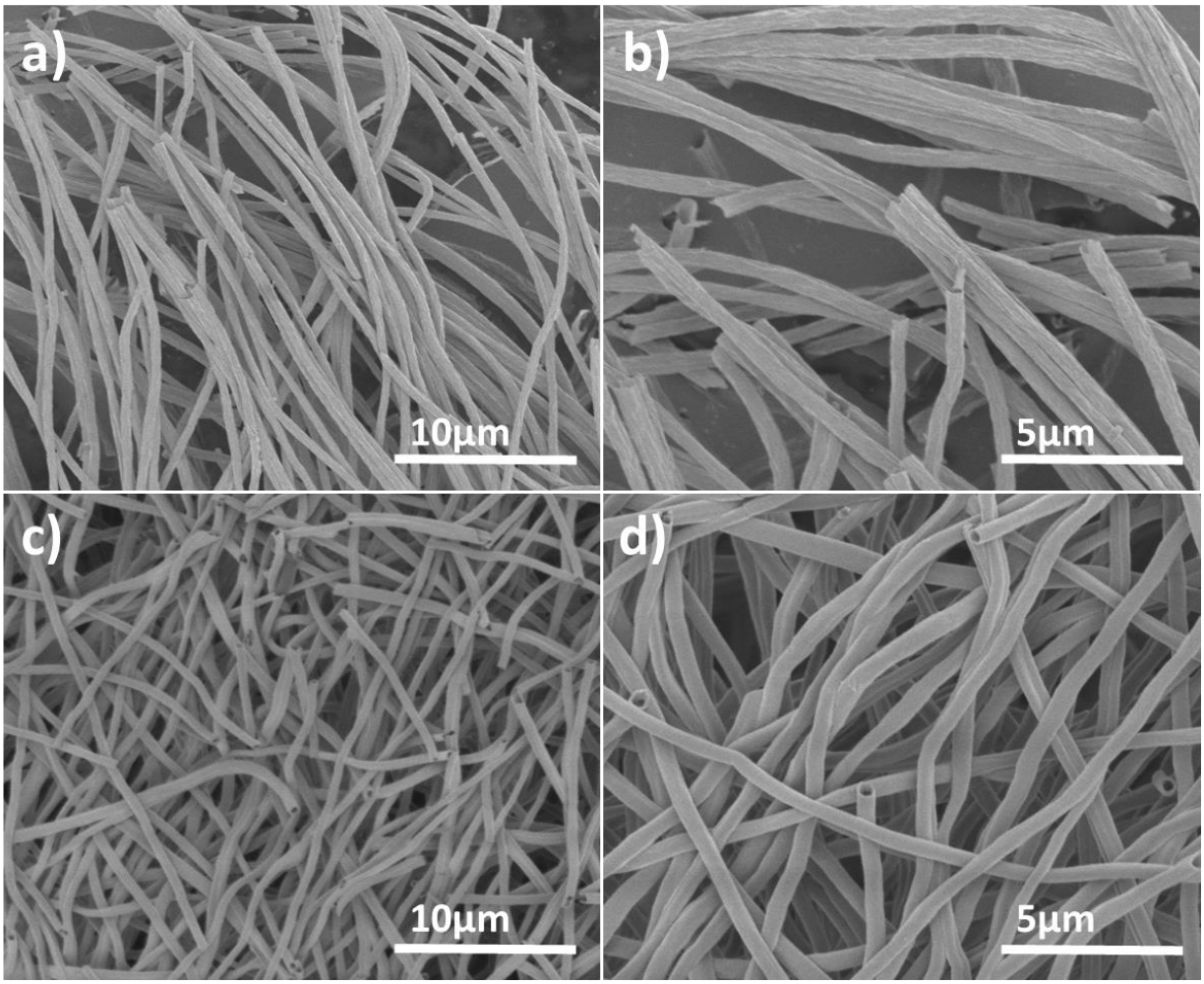

Figure 1: Scanning electron microscopy images a-b) d Al_2O_3 and c-d) p Al_2O_3.

To further understand the structure of prepared nanofibers, HRTEM was investigated. The TEM data confirmed the tubular structure of both samples that was also observed by SEM. It was found that p Al_2O_3 (Figure 2 b) and d Al_2O_3 (Figure 2 e) are both amorphous after annealing. Figure 2 a and S1 revealed the porous structure obtained after calcination of the deposited alucone layer on PAN NFs by MLD. Thus after the deposition of 50 cycles of alumina by ALD on PAN (figure 2 d-

e), dense structure was obtained after annealing under air. Contrary to ALD, MLD allows the formation of porous structure due to the TMA-EG layer. The calcination of the sample allow the elimination of the CH_2-CH_2 bond generated by ethylene glycol. Many parameters including the deposition thickness, the temperature ramp and temperature of calcination affect the porosity[34,38]. This structure allow a higher surface area than the dense alumina which will be confirmed by BET. Furthermore, Figure 2 c revealed the wall thickness of the tubular structure of p Al_2O_3 with a value of 69.8±4.2 nm compared to 27.7±4.7 nm in d Al_2O_3 (Figure 2 f).

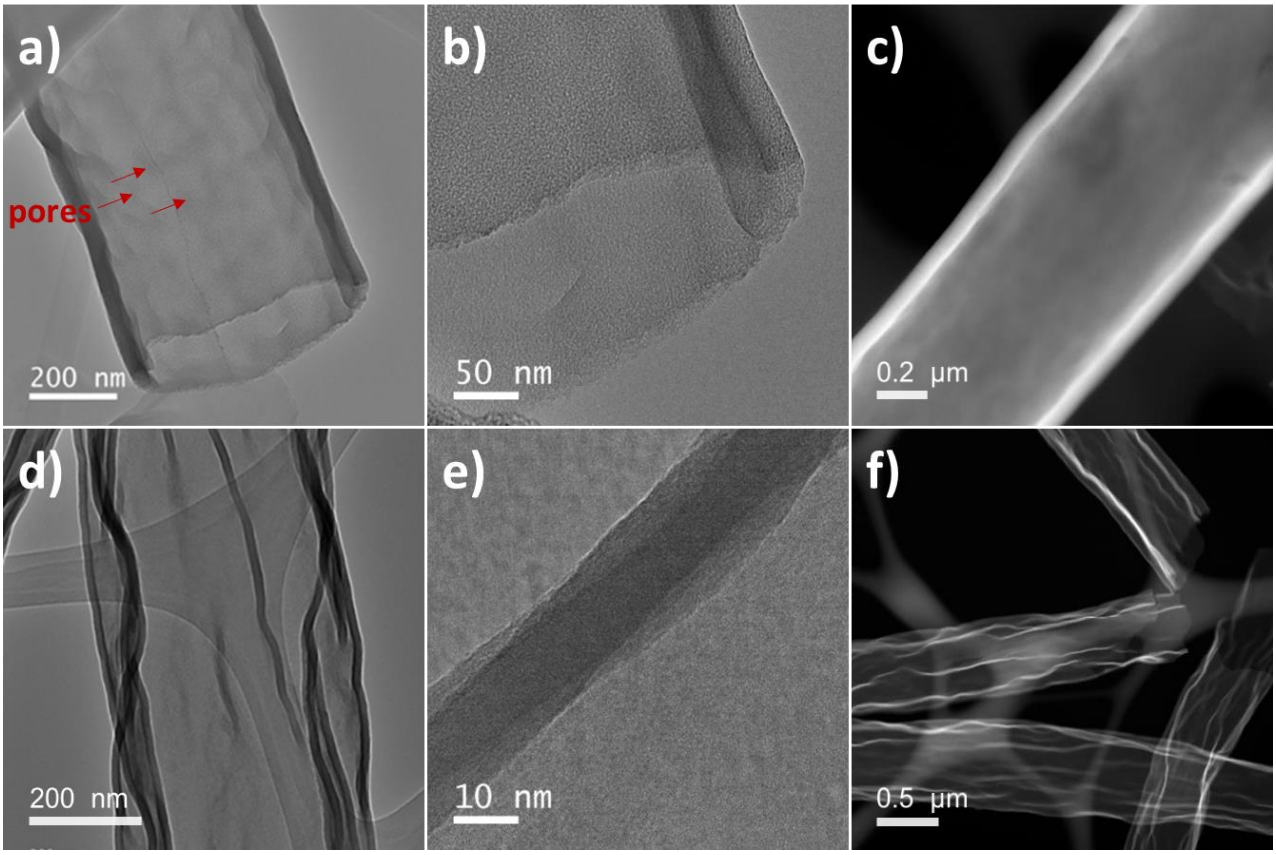

Figure 2: HRTEM image of a-c) p Al_2O_3 deposited by MLD and d-e) d Al_2O_3 deposited by ALD.

The X-Ray diffraction data confirm the amorphous structure found by HRTEM for both samples. Figure S2 shows that the calcination at 600°C did not affect the amorphous structure of the alumina nanofibers obtained by ALD and MLD

3.1.2 N_2 desorption/adsorption porosimetry (BET)

N_2 desorption/adsorption porosimetry was used to investigate the sample porosity. In this study, N_2 adsorption was considered to follow a type II isotherm model. The specific surface can be determined by exploiting the linear transformation of the BET isotherm. This analysis highlighted differences in the sorption curves of the **p Al_2O_3** and **d Al_2O_3** samples **(Figure 3).** The isotherm of the **p Al_2O_3** sample displayed a higher hysteresis loop from d **Al_2O_3** which could be explained by the presence of micropores and mesopores in the structure (**Figure 3a)**. Moreover, higher BET surface area was observed for the **p Al_2O_3** sample compared to the **d Al_2O_3** sample with 631.79 m^2/g for porous alumina and only 45.11 m^2/g for dense alumina. The surface area of micropores for p Al_2O_3 is calculated following t-plot model and the value obtained was 235.18 m^2/g. This indicates that the mesoporous structure is dominant in the porous Alumina sample. These results are in good agreement with HRTEM analysis. The alucone was converted after calcination to a porous structure with a high surface area that will play a major role in the adsorption mechanism of dyes.

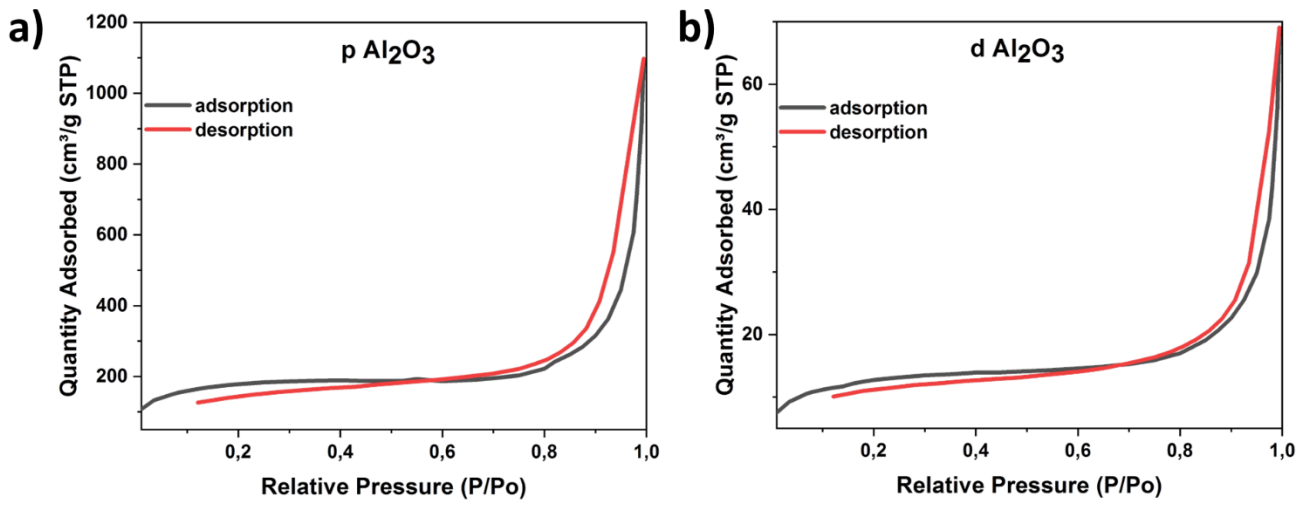

Figure 3: Nitrogen adsorption-desorption isotherms of (a) p Al_2O_3 and (b) d Al_2O_3 samples after calcination in air.

3.1.3 FTIR spectroscopy

The various functional groups present in the samples were identified by FTIR spectroscopy (**Figure 4)**. After calcination, all carbon content was burnt in the hybrid alucone polymeric films, as previously shown [39]. After calcination in air, the **p Al_2O_3** and **d Al_2O_3** samples showed very similar peaks in the FTIR spectra. This can be explained by alucone transformation into alumina nanofilms that have the same components as Al_2O_3 nanofilms after calcination. The peak range (800 to 950 cm^{-1}) indicated Al-O stretching vibrations, confirming the change from alucone hybrid material to alumina structure. The transmittance loss of the C-C and C-O stretching vibrations observed at 1132 and 1086 cm^{-1}, respectively, could be explained by thermal annealing. The small peak at 3300 cm^{-1} indicated O-H stretching vibrations.[40] A stretching vibration at 1205 cm^{-1} was previously reported and was due to methyl deformation of $AlCH_3$*.[41] An increase in transmittance associated with CH_2 asymmetric and symmetric stretching vibrations was observed at 2956 and 2870 cm^{-1}, respectively, corresponding to the stretching vibrations of the ethylene linkages between oxygen atoms in the aluminum alkoxide polymer.[32]

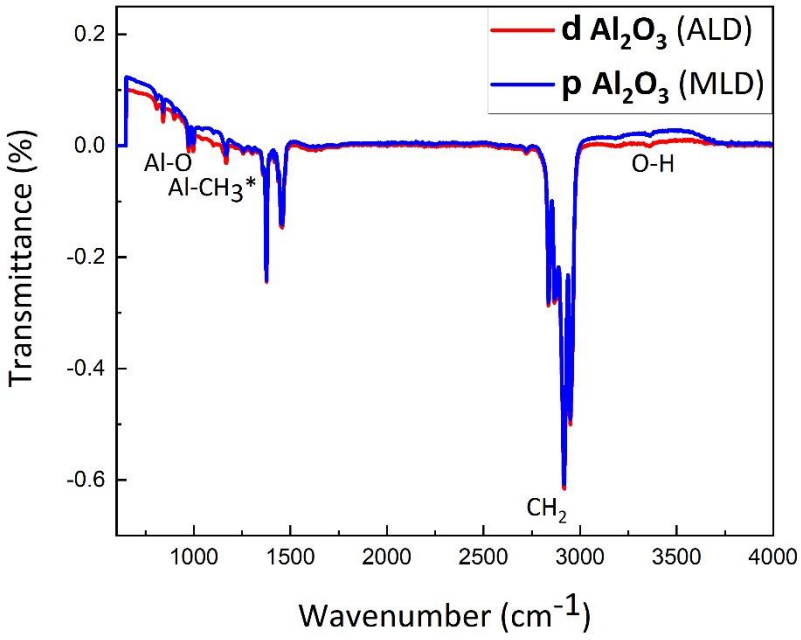

Figure 4: FTIR spectra of thin films deposited over PAN nanofibers: **d Al_2O_3** films (50 cycles of ALD) and **p Al_2O_3** films (250 cycles of MLD) after calcination

3.1.4 TGA analysis

Since trace of carbon were detected in FTIR, thermogravimetric analysis were conducted to further understand the stability of the elaborated samples. Figure 5a shows a total weight loss of almost 16% when the temperature was increased to 800°C under air. This could be attributed to the remaining CH_2 group detected in FTIR analysis due to the insufficient time of annealing or the adsorption of contaminants from air. For d Al_2O_3, a weight loss of only 3.0% (figure 5b) was observed. The weight loss of p Al_2O_3 was higher than the weight loss in d Al_2O_3 owing to the higher surface area of the porous sample that could adsorb more contaminants. The mass uptake in figure 6b of 1.2% between 600 and 800°C could be due to the oxidation of the sample at higher temperature as described elsewhere.[42]

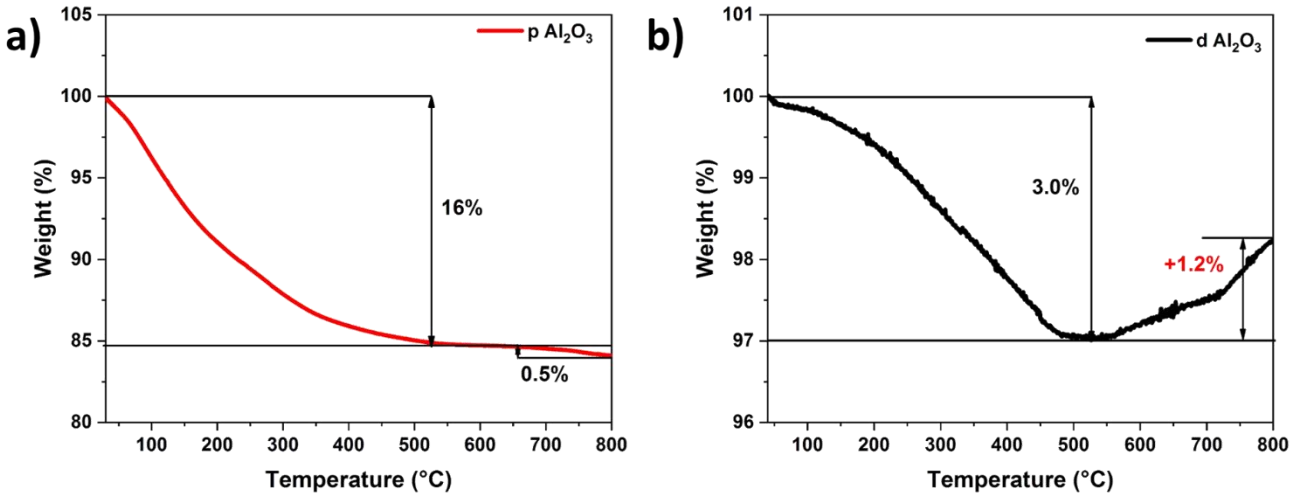

Figure 5: Thermogravimetric curve of a) p Al_2O_3 and b) d Al_2O_3

3.4 Adsorption activity

To better understand the absorption process, the adsorption of MB (i.e. organic pollutant dye) onto the prepared nanofibers (i.e. adsorbents) was monitored by UV/Vis spectrometry in view of potential applications for wastewater remediation.

3.4.1 MB adsorption onto p Al_2O_3 and d Al_2O_3 nanofibers

To measure the adsorption activity of **p Al_2O_3** and **d Al_2O_3** nanofibers after calcination in air, MB catalytic adsorption under UV light was monitored by UV/Vis spectrometry at different contact times (**Figure 6)**. The UV–Vis absorbance spectra shown in **Figure 6** of the MB solution displayed a main adsorption band at 664 nm permits to calculate the adsorption of MB dye using adsorption efficiency formula (**Equation 5**). The initial MB concentration was 10 ppm and the adsorbent concentration was 2 g/L (10mg of adsorbent in 5 mL of MB).

The adsorption efficiency was calculated as follows:

Adsorption efficiency (%) = (C_0 − C) /C_0 × 100. (**Equation 5**)

Where C_0 and C are the initial (before) and the final MB concentrations (after UV exposure).

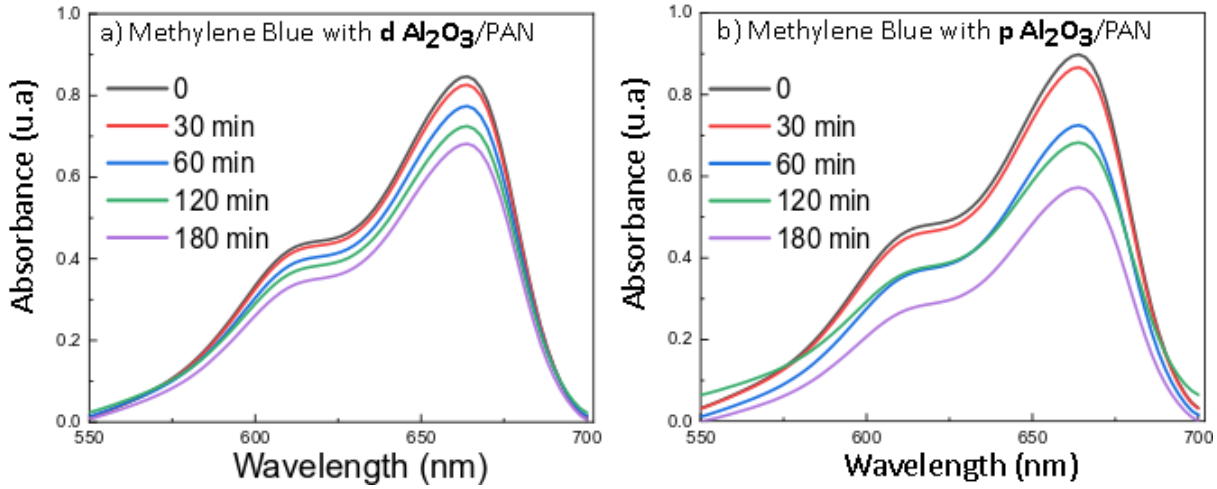

Figure 6: UV-Vis spectra of MB adsorption under UV light: a) **d Al_2O_3** and b) **p Al_2O_3**.

Comparison of the adsorption efficiency of the **d Al_2O_3** and **p Al_2O_3** samples in function of the dye-adsorbent contact time (**Figure 7**) showed that after 3 hours of contact time, the maximum efficiency was 22% for the **d Al_2O_3** and 30% for the **p Al_2O_3**. This indicates that the porous alumina structure prepared by MLD exhibits higher adsorption. Therefore, the next analyses concentrated only on the **p Al_2O_3** sample.

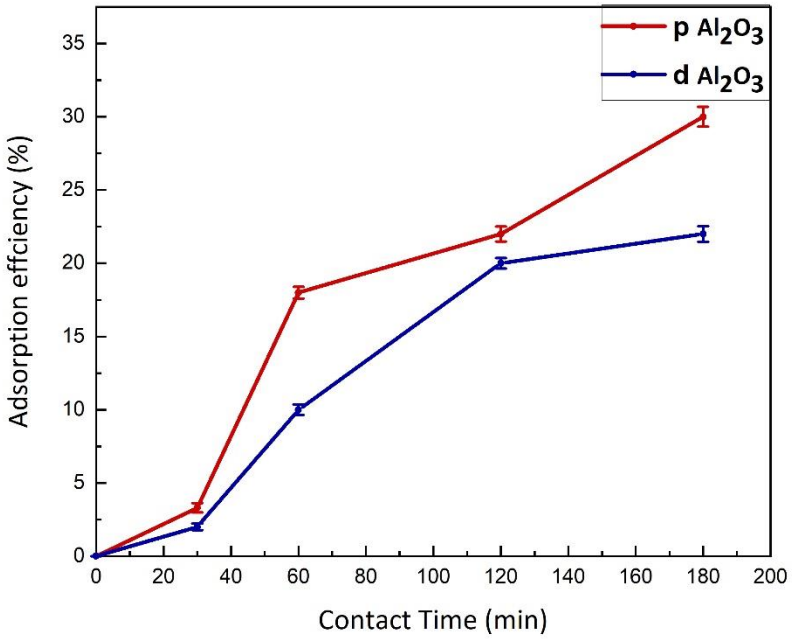

Figure 7: Adsorption efficiency of **d Al_2O_3** and **p Al_2O_3** nanofibers in function of the contact time between dye (5ppm of MB) and adsorbents.

3.4.2 Adsorption by p Al_2O_3 nanofibers

Due to the higher adsorption capacity of **p Al_2O_3** nanofibers, only the sample coated with alucone (250 cycles of MLD) was considered for the adsorption analysis. Different concentrations of MB (10, 7, 5, 3 and 1 ppm) with 4 g/L of **p Al_2O_3** nanofibers (20mg of adsorbents in 5 mL of MB) and various contact times (0, 30, 60, 120, 150 and 180 min) were used to compute the adsorption isotherms and kinetics.

a) Adsorption isotherms:

MB adsorption onto **p Al_2O_3** nanofibers was quantitatively described using the Langmuir and Freundlich linear models, (Figure 8 a-b). **Table 1** shows the adsorption parameters for the two models, calculated using Equations (1) and (2), and the correlation coefficient R^2 of the fitting. The R^2 value was higher with the Langmuir (Figure 8a) than with the Freundlich model (Figure 8b)

(0.999 and 0.958). This indicates that MB adsorption onto porous alumina is better described by the Langmuir model (i.e. monolayer adsorption process on the adsorbent homogeneous surface, without considering the interaction between adsorbate molecules).

Table 1. Adsorption isotherm parameters for MB adsorption using the Langmuir and Freundlich linear models.

Model	Parameters	Value
Langmuir	q_{max} (mg/g)	0.965 ± 0.002
	k_L (L/mg)	1.869 ± 0.005
	R_L	0.014 - 0.25
	R^2	0.999
Freundlich	k_F ((mg/g)(L/mg)$^{1/n}$)	0.75
	N	2.767
	R^2	0.958

b) Adsorption kinetics

The relationship between adsorbed quantity and sorption time was described using pseudo first-order and pseudo second-order kinetic models (Figure 8 c-d), and the adsorption parameters and R^2 were calculated using Equations (3) and (4) (**Table 2**). The control experiments for adsorption of MB onto **p Al_2O_3** nanofibers were carried out in the same experimental conditions, simultaneously.

Table 2. Adsorption kinetic parameters for MB adsorption onto **p Al_2O_3** nanofibers calculated with the pseudo first-order and pseudo second-order kinetic models.

Model	Parameters	Values
Pseudo first-order	qe (cal) (mg/g)	1.3
	K_1(1/min)*10^{-4}	9.9
	R^2	0.99
Pseudo second-order	qe (cal) (mg/g)	1.5
	K_2(g/(mg_min))*10^{-4}	6.2
	R^2	0.26

Figure 8c-d and **Table 2** clearly indicated that the experimental data are better described by the pseudo first-order than the pseudo second-order kinetic model (R^2: 0.999 and 0.26, respectively) and that the reaction is mostly explained by physisorption.

Ho and McKay found that most adsorbents in aqueous solutions show pseudo second-order kinetics, especially for long sorption times[43]. Conversely, MB adsorption onto porous alumina nanofibers did not behave like most of the previously investigated sorption processes in water due to the difference in dye and adsorbent concentration.

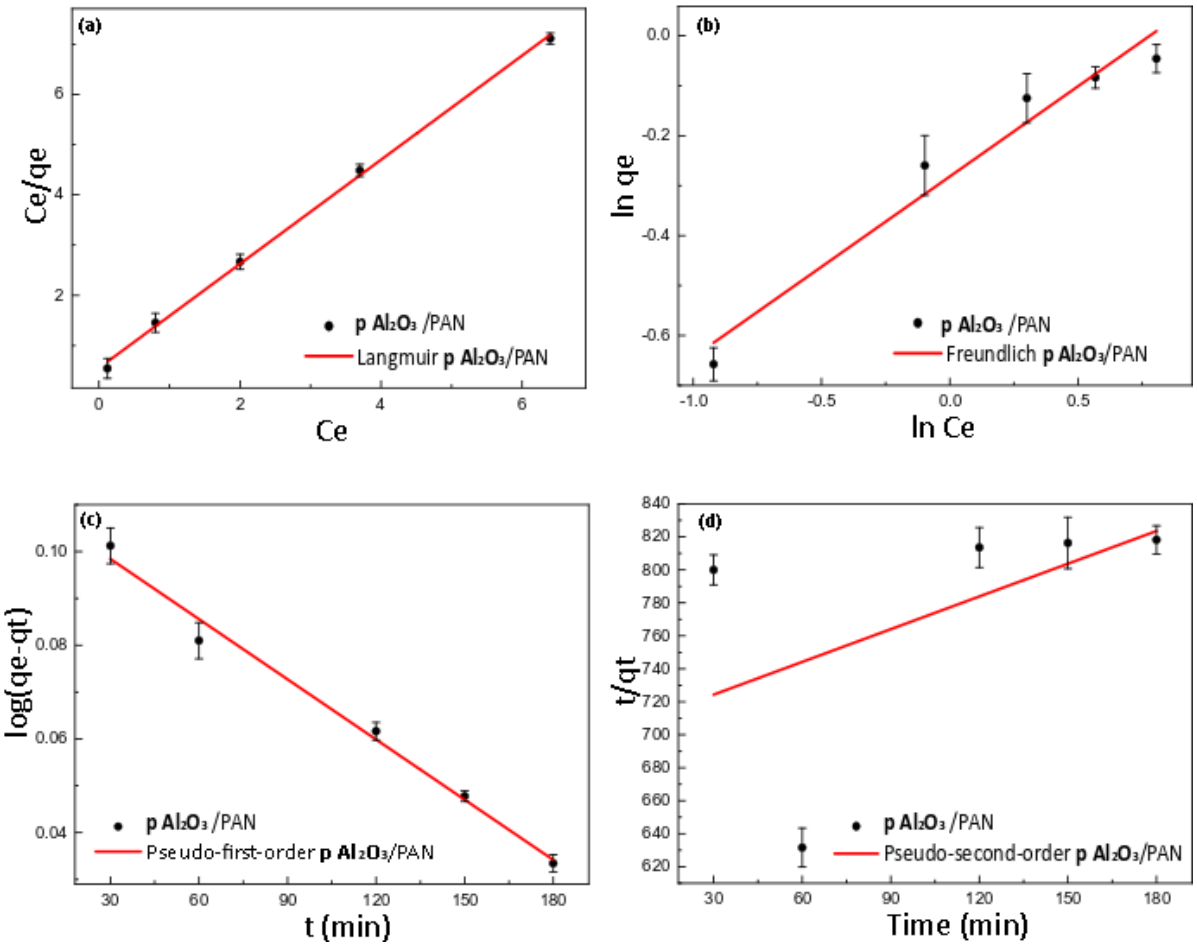

Figure 8: Isotherms calculated with the Langmuir (a), and Freundlich (b) linear models for MB adsorption onto the p Al_2O_3 nanofibers after 3 hours of contact. Kinetics calculated with the pseudo first-order (c) and pseudo second-order (d) kinetic models during 3 hours.

Compared with the results of previous studies on dye-adsorption capacities (**Table 3**), porous alumina nanofibers displayed high adsorption (88%) using a small amount of adsorbents. This is an improvement of the competitive efficiency of hybrid materials, and shows MLD suitability for the fabrication of dye adsorbents. Moreover, recyclability of the adsorbent and the mechanism of adsorption were also been discussed in the following paragraph.

Table 3. Comparison of the dye adsorption performances of different adsorbents

Adsorbent	Dye	pH range	% removal	Reference
Modified-Alumina	Crystal violet	2.6–10.8	80	[44]
Activated clay	Methylene blue	2–9	95	[45]
Kaolin	Crystal violet	2–7	95	[46]
Activated rice husk	Acid yellow 36	2–9	45	[47]
Fly ash	Methylene blue	2–8	45	[48]
Pine leaves	Methylene blue	2–11	80	[49]
Fe_2O_3	Acid red 27	1.5–10.5	98	[50]
Pine cone	Congo red	3.55–10.95	60.5	[51]
Pine cone	Methylene blue	3.47–7.28	94.82	[52]
Tobacco Stem Ash	Methylene blue	2.08–7.93	81	[53]
Alucone	Methylene blue	3–9	88	this work

c) Recyclability and mechanism of adsorption

The MB is a cationic dye in pH =9 [54–56] which has the ability to attach with the Al_2O_3 negative surface [57]. The presence of Al_2O_3 on the surface of nanofibers enhanced the charge distribution of porous adsorbents.

Furthermore, the p Al_2O_3 nanofibers have ability to be reused for several cycles (at least 5 cycles) without losing their efficiency as presented in Figure 9.

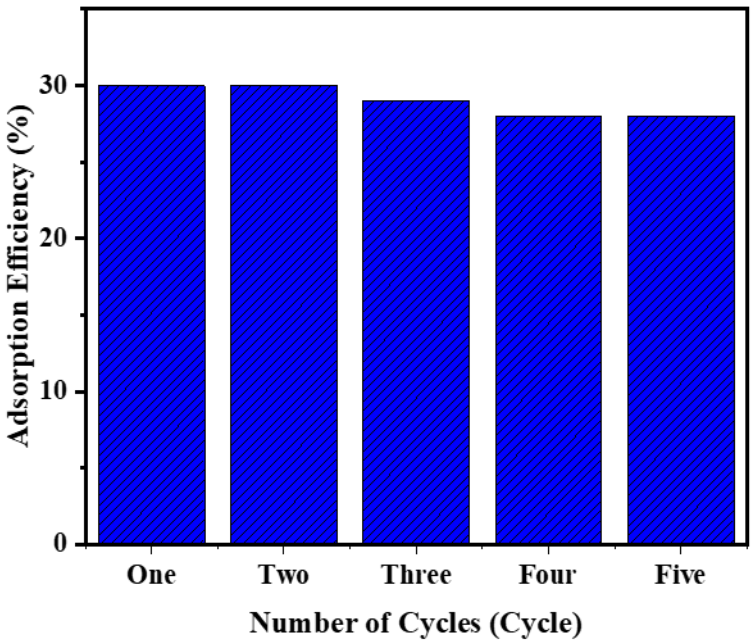

Figure 9: The adsorption efficiency of p Al_2O_3 as catalysts for removal of MB throughout five consecutive cycles of filtration and reuse.

Several probable adsorption mechanisms such as hydrogen bonding, electrostatic interaction, ion exchange, acid-base interaction, coordination, have been proposed to realize the interactions between solid adsorbent and MB dye molecules in an aqueous solution. In this present work, as a cationic organic molecule [54,56,58], MB was adsorbed onto the surface of prepared porous Al_2O_3 mainly through electrostatic interaction and hydrogen bonding. This can be explained by the presence of high amount of Al–OH and Al–O groups on the adsorbent surface. The adsorption capacity increases with increasing the pH of the MB solution, suggesting that more deprotonated Al–OH groups exist in the form of $Al–O^-$ [57], which possess stronger electrostatic interaction with cationic dye MB. In addition, the Al–OH group on the surface of the prepared p Al_2O_3 can also interact with the amine group of MB molecule via hydrogen bonding as has been reported for other mesoporous materials [59]. Therefore, the adsorption mechanisms can be interpreted by electrostatic interaction and hydrogen bonding (Figure 10).

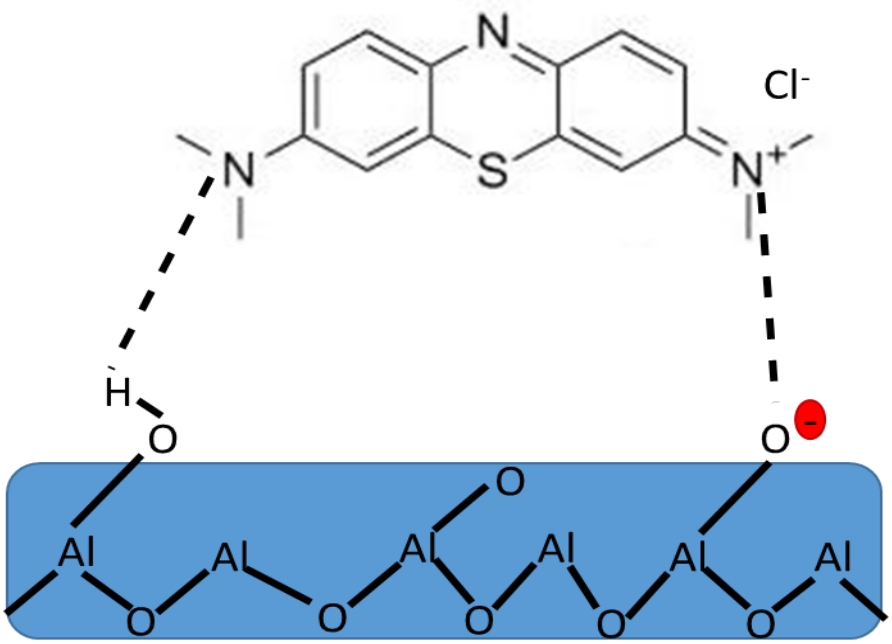

Figure 10: The adsorption efficiency of p Al_2O_3 as catalysts for removal of MB throughout five consecutive cycles of filtration and reuse.

Conclusion

Improving the nanomaterial adsorption performance for wastewater remediation is still a challenging task. In this work, we designed and prepared highly efficient nanomaterials by coating PAN nanofibers using MLD. The calcination in air of ''alucone'' hybrid polymeric thin films prepared by MLD allowed the conversion of the hybrid structure into an alumina mesoporous structure. The high porosity and large surface area (631.7 m^2/g) explain the high MB adsorption efficiency (88%). Moreover, the adsorption isotherms calculated with the Langmuir model showed that MB adsorption onto porous alumina nanofibers is a monolayer adsorption process (physical adsorption). The present results highlight the potential of nanomaterials coated by MLD for organic dye removal and water pollution remediation.

Acknowledgments

This study was financially supported by the French National Agency (ANR, program MeNiNA-ANR-17-CE09-0049). The authors would also like to acknowledge the partial financial support from the National Science Centre (NCN) of Poland by the SONATA BIS grant 2020/38/E/ST5/00176 and the OPUS grant 2019/35/B/ST5/00248, respectively.

References

1. Ismail, M. *et al.* Pollution, Toxicity and Carcinogenicity of Organic Dyes and their Catalytic Bio-Remediation. *Curr. Pharm. Des.* **25**, 3645–3663 (2019).

2. Kazancioglu, E. O., Aydin, M. & Arsu, N. Photochemical synthesis of nanocomposite thin films containing silver and gold nanoparticles with 2-thioxanthone thioacetic acid-dioxide and their role in photocatalytic degradation of methylene blue. *Surfaces and Interfaces* **22**, 100793 (2021).

3. Weber, M., Julbe, A., Ayral, A., Miele, P. & Bechelany, M. Atomic Layer Deposition for Membranes: Basics, Challenges, and Opportunities. *Chem. Mater.* **30**, 7368–7390 (2018).

4. El-maghrabi, H. H., Ahmed, E., Soliman, F. S., Mohamed, Y. & Amin, A. E. One pot environmental friendly nanocomposite synthesis of novel TiO_2 -nanotubes on graphene sheets as effective photocatalyst. *Egypt. J. Pet.* **25**, 575–584 (2016).

5. Gupta, V. K. & Saleh, T. A. Sorption of pollutants by porous carbon , carbon nanotubes and fullerene - An overview. 2828–2843 (2013) doi:10.1007/s11356-013-1524-1.

6. Carmen, Z. & Daniela, S. Textile Organic Dyes – Characteristics , Polluting Effects and Separation / Elimination Procedures from Industrial Effluents – A Critical Overview. (2010).

7. Medhat, A. *et al.* Efficiently activated carbons from corn cob for methylene blue adsorption. *Appl. Surf. Sci. Adv.* **3**, 100037 (2021).

8. Van Bui, H., Grillo, F. & Van Ommen, J. R. Atomic and molecular layer deposition: off the beaten track. *Chem. Commun.* **53**, 45–71 (2017).

9. Van De Kerckhove, K. *et al.* The transformation behaviour of 'alucones', deposited by molecular layer deposition, in nanoporous Al 2 O 3 layers. *Dalt. Trans.* **47**, 5860–5870 (2018).

10. El-Sayed, M. & Nada, A. A. Polyethylenimine −functionalized amorphous carbon fabricated from oil palm leaves as a novel adsorbent for Cr(VI) and Pb(II) from aqueous solution. *J. Water Process Eng.* (2017) doi:10.1016/j.jwpe.2017.02.012.

11. El-Maghrabi, H. H. *et al.* Magnetic graphene based nanocomposite for uranium scavenging. *J. Hazard. Mater.* **322**, (2017).

12. Barhoum, A. *et al.* Nanofibers as new-generation materials : From spinning and nano-spinning fabrication techniques to emerging applications. *Appl. Mater. Today* **17**, 1–35 (2019).

13. Said, S., Mikhail, S. & Riad, M. Recent progress in preparations and applications of meso-porous alumina. *Mater. Sci. Energy Technol.* **2**, 288–297 (2019).

14. Soni, B. S. S., Henderson, M. J. & Gibaud, A. Visible-Light Photocatalysis in Titania-Based Mesoporous Thin Films **. 1493–1498 (2008) doi:10.1002/adma.200701066.

15. Shen, S. C. *et al.* Solid-based hydrothermal synthesis and characterization of alumina nanofibers with controllable aspect ratios. *J. Am. Ceram. Soc.* **92**, 1311–1316 (2009).

16. Ma, M. G. & Zhu, J. F. A facile solvothermal route to synthesis of γ-alumina with bundle-like and flower-like morphologies. *Materials Letters* vol. 63 881–883 (2009).

17. Jagminas, A., Kuzmarskyte, J., Malferrari, L. & Cuffiani, M. A new route of alumina template modification into dense-packed fibrilous material. *Mater. Lett.* **61**, 2896–2899 (2007).

18. Yu, P. C., Yang, R. J., Tsai, Y. Y., Sigmund, W. & Yen, F. S. Growth mechanism of single-crystal α-Al2O3 nanofibers fabricated by electrospinning techniques. *J. Eur. Ceram. Soc.* **31**, 723–731 (2011).

19. Vahtrus, M. *et al.* Mechanical and structural characterizations of gamma- and alpha-alumina nanofibers. *Mater. Charact.* **107**, 119–124 (2015).

20. Najem, M. *et al.* Palladium/carbon nanofibers by combining atomic layer deposition and electrospinning for organic pollutant degradation. *Materials (Basel).* **13**, 1–18 (2020).

21. Shi, Q. *et al.* Durable antibacterial Ag/polyacrylonitrile (Ag/PAN) hybrid nanofibers prepared by atmospheric plasma treatment and electrospinning. *Eur. Polym. J.* **47**, 1402–1409 (2011).

22. Salameh, C., Eid, C. & Bechelany, M. Palladium / Carbon Nanofibers by Combining Atomic Layer Deposition and Electrospinning for Organic Pollutant Degradation. 1–18.

23. Celebioglu, A., Ranjith, K. S., Eren, H., Biyikli, N. & Uyar, T. Surface decoration of pt nanoparticles via ALD with TiO2 protective layer on polymeric nanofibers as flexible and reusable heterogeneous nanocatalysts. *Sci. Rep.* **7**, 1–10 (2017).

24. Park, K. *et al.* Effects of atomic layer deposition conditions on the formation of thin ZnO films and their photocatalytic characteristics. *Ceram. Int.* **45**, 18823–18830 (2019).

25. George, S. M. Atomic layer deposition: An overview. *Chem. Rev.* **110**, 111–131 (2010).

26. Weber, M., Julbe, A., Kim, S. S. & Bechelany, M. Atomic layer deposition (ALD) on inorganic or polymeric membranes. *J. Appl. Phys.* **126**, (2019).

27. Merenda, A. *et al.* Fabrication of Pd-TiO 2 nanotube photoactive junctions via Atomic Layer Deposition for persistent pesticide pollutants degradation. *Appl. Surf. Sci.* **483**, 219–230 (2019).

28. Ghazaryan, L., Kley, E.-B., Tünnermann, A. & Viorica Szeghalmi, A. Stability and annealing of alucones and alucone alloys. *J. Vac. Sci. Technol. A Vacuum, Surfaces, Film.* **31**, 01A149 (2012).

29. Weber, M. *et al.* Novel and Facile Route for the Synthesis of Tunable Boron Nitride Nanotubes Combining Atomic Layer Deposition and Annealing Processes for Water Purification. *Advanced Materials Interfaces* vol. 5 (2018).

30. Meng, X. An overview of molecular layer deposition for organic and organic-inorganic hybrid materials: Mechanisms, growth characteristics, and promising applications. *J. Mater. Chem. A* **5**, 18326–18378 (2017).

31. Chronakis, I. S. Novel nanocomposites and nanoceramics based on polymer nanofibers using electrospinning process - A review. *J. Mater. Process. Technol.* **167**, 283–293 (2005).

32. Dameron, A., a. *et al.* Molecular Layer Deposition of Alucone Polymer Films Using Trimethylaluminum and Ethylene Glycol. *Chem. Mater.* **20**, 3315–3326 (2008).

33. Choudhury, D., Sarkar, S. K. & Mahuli, N. Molecular layer deposition of alucone films using trimethylaluminum and hydroquinone. *J. Vac. Sci. Technol. A Vacuum, Surfaces, Film.* **33**, 01A115 (2014).

34. Sayegh, S. *et al.* Humidity-resistant gas sensors based on SnO2 nanowires coated with a porous alumina nanomembrane by molecular layer deposition. *Sensors Actuators B Chem.* **344**, 130302 (2021).

35. Viter, R., Chaaya, A. A. & Iatsunskyi, I. Tuning of ZnO 1D nanostructures by atomic layer deposition and electrospinning for optical gas sensor applications. *Nanotechnology* **26**, 105501 (2015).

36. Elias, J. *et al.* Electrochimica Acta Electrochemical growth of ZnO nanowires on atomic layer deposition coated polystyrene sphere templates. *Electrochim. Acta* **110**, 387–392 (2013).

37. Nada, A. A., Bekheet, M. F., Roualdes, S., Gurlo, A. & Ayral, A. Functionalization of MCM-41 with titanium oxynitride deposited via PECVD for enhanced removal of methylene blue. *J. Mol. Liq.* **274**, 505–515 (2019).

38. Zhang, L. *et al.* Nano Energy Rational design of porous structures via molecular layer

deposition as an effective stabilizer for enhancing Pt ORR performance. *Nano Energy* **60**, 111–118 (2019).

39. Liang, X. & Weimer, A. W. An overview of highly porous oxide films with tunable thickness prepared by molecular layer deposition. *Curr. Opin. Solid State Mater. Sci.* **19**, 115–125 (2015).

40. Liang, X., Yu, M., Li, J., Jiang, Y. B. & Weimer, A. W. Ultra-thin microporous-mesoporous metal oxide films prepared by molecular layer deposition (MLD). *Chem. Commun.* 7140–7142 (2009) doi:10.1039/b911888h.

41. Lee, B. H., Yoon, B., Anderson, V. R. & George, S. M. Alucone alloys with tunable properties using alucone molecular layer deposition and Al 2O 3 atomic layer deposition. *J. Phys. Chem. C* **116**, 3250–3257 (2012).

42. Aumann, C. E. *et al.* Oxidation behavior of aluminum nanopowders Oxidation behavior of aluminum nanopowders. **1178**, (2014).

43. Jia, X. J. *et al.* Bouquet-like calcium sulfate dihydrate: A highly efficient adsorbent for Congo red dye. *RSC Adv.* **5**, 72321–72330 (2015).

44. Adak, A., Bandyopadhyay, M. & Pal, A. Removal of crystal violet dye from wastewater by surfactant-modified alumina. *Sep. Purif. Technol.* **44**, 139–144 (2005).

45. Fu, Y. & Viraraghavan, T. Removal of Congo Red from an aqueous solution by fungus Aspergillus niger. *Adv. Environ. Res.* **7**, 239–247 (2002).

46. Nandi, B. K., Goswami, A., Das, A. K., Mondal, B. & Purkait, M. K. Kinetic and equilibrium studies on the adsorption of crystal violet dye using Kaolin as an adsorbent. *Sep. Sci. Technol.* **43**, 1382–1403 (2008).

47. Hameed, B. H. & Ahmad, A. L. Aqueous-Phase Adsorption of Phenolic Compounds on Activated Carbon. *Langmuir* 630–635 (2003).

48. Kumar, K. V., Ramamurthi, V. & Sivanesan, S. Modeling the mechanism involved during the sorption of methylene blue onto fly ash. *J. Colloid Interface Sci.* **284**, 14–21 (2005).

49. Yagub, M. T., Sen, T. K. & Ang, H. M. Equilibrium, kinetics, and thermodynamics of methylene blue adsorption by pine tree leaves. *Water. Air. Soil Pollut.* **223**, 5267–5282 (2012).

50. Nassar, N. N. Kinetics, mechanistic, equilibrium, and thermodynamic studies on the adsorption of acid red dye from wastewater by γ-Fe2O3 nanoadsorbents. *Sep. Sci. Technol.* **45**, 1092–1103 (2010).

51. Dawood, S. & Sen, T. K. Removal of anionic dye Congo red from aqueous solution by raw

pine and acid-treated pine cone powder as adsorbent: equilibrium, thermodynamic, kinetics, mechanism and process design. *Water Res.* **46**, 1933–46 (2012).

52. Sen, T. K., Afroze, S. & Ang, H. M. Equilibrium, kinetics and mechanism of removal of methylene blue from aqueous solution by adsorption onto pine cone biomass of Pinus radiata. *Water. Air. Soil Pollut.* **218**, 499–515 (2011).

53. Ghosh, R. K. & Reddy, D. D. Tobacco stem ash as an adsorbent for removal of methylene blue from aqueous solution: Equilibrium, kinetics, and mechanism of adsorption. *Water. Air. Soil Pollut.* **224**, (2013).

54. Biswas, S., Rashid, T. U., Debnath, T. & Haque, P. Application of Chitosan-Clay Biocomposite Beads for Removal of Heavy Metal and Dye from Industrial E ffl uent. 1–14 (2020).

55. Nsenga, M. & Li, X. Environmental Technology & Innovation Large-scale hybrid accidental urban wetland for polluted river purification in northern China : Evidence and implications for urban river management. *Environ. Technol. Innov.* **22**, 101542 (2021).

56. Elshypany, R. *et al.* Magnetic ZnO Crystal Nanoparticle Growth on Reduced Graphene Oxide for Enhanced Photocatalytic Performance under Visible Light Irradiation. (2021).

57. Al, O. & Al, Y. O. Charge conversion and mass transfer on surface of. 4335–4340 (2013) doi:10.1039/c3ce27026b.

58. Elshypany, R. *et al.* Elaboration of Fe3O4/ZnO nanocomposite with highly performance photocatalytic activity for degradation methylene blue under visible light irradiation. *Environ. Technol. Innov.* **23**, 101710 (2021).

59. Yuan, N., Cai, H., Liu, T., Huang, Q. & Zhang, X. Adsorptive removal of methylene blue from aqueous solution using coal fly ash-derived mesoporous silica material. *Adsorpt. Sci. Technol.* **37**, 333–348 (2019).